[redacted] UNCLASSIFIED

LA-5658

C. 3

Reporting Date: June 1974
Issued: September 1974

PHERMEX Evaluation of Air Force Tungsten and U-0.75 wt% Ti Penetrators (U)

by

L. W. Hantel
J. W. Taylor

los alamos
scientific laboratory
of the University of California
LOS ALAMOS, NEW MEXICO 87544

[redacted]

[redacted] UNCLASSIFIED

Work supported by Air Force Armament Laboratory, Air Force Systems Command, Eglin Air Force Base, FL.

[redacted]

PHERMEX EVALUATION OF AIR FORCE TUNGSTEN AND U-0.75 Wt% Ti PENETRATORS

by

L. W. Hantel and J. W. Taylor

ABSTRACT (U)

The LASL PHERMEX machine was used to radiograph the interaction of tungsten and two hardnesses of uranium-0.75 wt% titanium penetrators with MIL-S-13812A armor plate at 45° obliquity. Multiple firings permitted penetration-time histories of both penetration and nonpenetration shots to be observed.

Penetration trajectory plots made from the radiographs and the detailed shapes of the penetrators midway through the penetration process lead to several interesting conclusions. In general, the penetration process begins with a stage in which hydrodynamic forces govern and the penetrator is eroded rapidly, followed by a stage during which the residual kinetic energy of the penetrator punches a plug out of the armor.

The tungsten alloy's relatively high ductility is self-defeating because the penetrator presents too broad a frontal area to the armor. The softer U-0.75 wt% Ti alloy produces a larger fragment behind the armor than the harder alloy, apparently because the latter fragments catastrophically at late times.

The uranium alloys, in contrast to the tungsten, bend markedly during penetration, apparently because of their lower elastic modulus and Hugoniot elastic limits. These effects are accentuated by the present penetrator design.

Metallography of these U-0.75 wt% Ti penetrators revealed centerline quenching voids.

I. INTRODUCTION

The Los Alamos Scientific Laboratory (LASL), under an agreement with the Air Force Armament Laboratory (AFATL), Air Force Systems Command, Eglin Air Force Base, performed a detailed study to determine what uranium alloy would be the best penetrator material for use in a proposed 30-mm gun system.[1] As part of that study, the LASL high-intensity 28-MeV PHERMEX flash x-ray facility was used to radiograph the penetrator-armor interaction through 152 mm of steel. The radiographs showed that during penetration, projectile deformation was confined to a relatively narrow region next to the penetrator-armor interface. The deformation consisted of rapid radial displacement of the penetrator material starting at the moment of impact and continuing until a plug was sheared out of the armor or the projectile was defeated. The displaced penetrator material adhered to the walls of the hole, and the rest of the penetrator proceeded essentially undeformed. This unusual behavior was attributed to the low propagation velocity of stress waves in uranium

1. J. W. Hopson, L. W. Hantel, and D. J. Sandstrom, "Evaluation of Depleted-Uranium Alloys for Use in Armor-Piercing Projectiles," Los Alamos Scientific Laboratory report LA-5238 (1973).

which requires far too long a time for significant penetrator deformation outside the interaction zone.

Since our first report,[1] AFATL has proceeded with a vigorous program to increase penetration by redesigning the penetrator. AFATL has evaluated several penetrator designs, and one of the most promising is that examined in this program. The projectile tested is shown in Fig. 1. AFATL tests showed that penetrators of this design penetrated better than other designs tested. However, for the past few months AFATL has experienced difficulty in reproducing these results. Hence, AFATL asked us to examine the penetrator-armor interaction with our 28-MeV PHERMEX machine. In particular, we would look for premature core failure and examine entrance and exit hole angles, core deflection during penetration, and core integrity behind the armor. We were also asked for complete chemical and metallurgical analysis of both U-0.75 wt% Ti alloys.

II. EXPERIMENTAL

The experimental program consisted of firing the penetrators into 50.4-mm-thick by 152-mm-wide by 304-mm-long MIL-S-13812A armor plate at 45° obliquity and radiographing the penetrator-armor interaction. Two U-0.75 wt% Ti hardnesses (46-47 R_c and 53-54 R_c) and W-2 Kennertium tungsten alloy were evaluated. All three materials were fired at an incident velocity sufficient to penetrate the armor, and the 53-54 R_c uranium alloy was also fired at a velocity insufficient to penetrate the armor. Several shots were fired with each material, allowing radiographs to be taken at various penetration depths. A 5-mm-thick 2024 T-3 aluminum witness plate 152 mm behind the armor verified penetration or nonpenetration by each shot.

The 30-mm rifle used for these tests was built by Mathewson Tool Company according to G. W. Amron drawings. Because our rifle barrel has a different twist and chamber from that used by AFATL, we had to fire a number of preliminary shots to establish the powder loads necessary to produce the penetration and nonpenetration shots and to be sure that this projectile was stable in flight when launched from our rifle. In all, we fired 22 preliminary shots against 50.4-mm-thick by 304-mm-square MIL-S-13812A armor plate at 45° obliquity. We took orthogonal x rays of each shot to determine the yaw angle and projectile integrity at the target. As received, these projectiles would not chamber in our rifle. However, by machining about 4.75 mm off the front of the nylon driving band, we could make the round chamber properly, and yaw at the target was held to less than 1° in each plane. Table I lists the loads and velocities selected for the PHERMEX shots. Although these loads were conservative on the basis of the preliminary shots, when we began to fire in front of PHERMEX we found that the projectiles were not so reproducible as we thought, so the armor defeated some projectiles whose velocities were expected to cause penetration. Because we had only a limited number of each type of penetrator, we increased the powder load to ensure obtaining our penetration sequence. The velocity was increased only a few meters per second.

Timing for the radiographs was accomplished with a "make" foil attached to the front of the armor plate

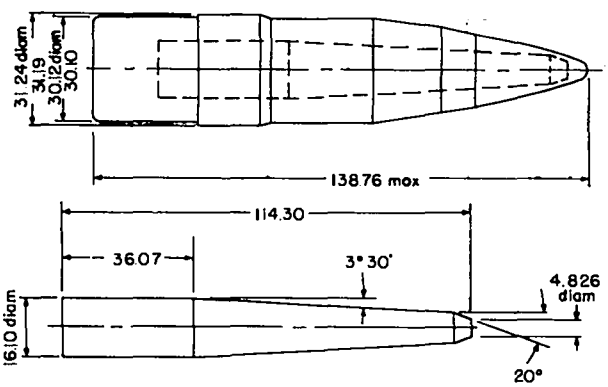

Fig. 1.
Thirty-mm HD API projectile (dimensions in millimeters).

TABLE I

POWDER LOADS AND VELOCITIES FOR PHERMEX SHOTS

Material	Load (g CIL-1379C)	Velocity (m/sec)
Penetration Series		
Hard U-0.75 wt% Ti	148	945
Soft U-0.75 wt% Ti	148	945
W-2 Tungsten	155	975
Nonpenetration Series		
Hard U-0.75 wt% Ti	140	899

target. When the projectile penetrated this foil, an electrical circuit was completed, giving us a "zero time" signal. This signal was then delayed to trigger PHERMEX at the desired time. The foil was two layers of 0.127-mm-thick copper shim stock separated by a layer of tissue paper. Figure 2 shows the circuit used.

III. RESULTS

A. PHERMEX Shots

The penetration shots with tungsten alloy penetrators gave seven radiographs at delays of 20, 50, 100, 150, 200, 275, and 325 μs. These radiographs are shown as Fig. 3.

The penetration shots with hard U-0.75 wt% Ti gave six radiographs at delays of 50, 100, 150, 275, 325, and 421 μs, shown as Fig. 4. The nonpenetration shots with this material gave four radiographs at delays of 20, 100, 150, and 250 μs, shown as Fig. 5.

The penetration shots with soft U-0.75 wt% Ti gave five radiographs at delays of 50, 100, 150, 275, and 325 μs, shown as Fig. 6. In addition, a nonpenetration shot at 100-μs delay is shown as Fig. 7.

The most striking observation in these tests was the bending of the uranium alloy penetrators. This is shown clearly in Fig. 4b, the 100-μs-delay penetration shot with hard U-0.75 wt% Ti. This amount of bending was typical of the uranium alloy penetrators. The rear of the penetrator is still at 45° obliquity to the plate while the part inside the armor is at about 56° obliquity. This difference ultimately results in the curved penetration path shown in Fig. 6e, the 325-μs-delay penetration shot with soft U-0.75 wt% Ti. In contrast, Fig. 3c shows the 100-μs-delay tungsten penetration shot. Here the penetrator is proceeding normally with no tendency to bend. This difference in behavior can be ascribed to the fact that the tungsten alloy's elastic modulus is about twice that of the uranium alloy so it can resist the bending stresses caused by the 45°-obliquity striking angle. Adding to this problem is the present penetrator design that tends to increase the stress component perpendicular to the penetrator axis. The first penetrator design tested at LASL[1] was a right circular cylinder except for the very tip, and PHERMEX radiographs show it penetrating armor at 60° obliquity without bending, despite this severer condition. It seems appropriate to suggest that the penetrator be redesigned with this in mind.

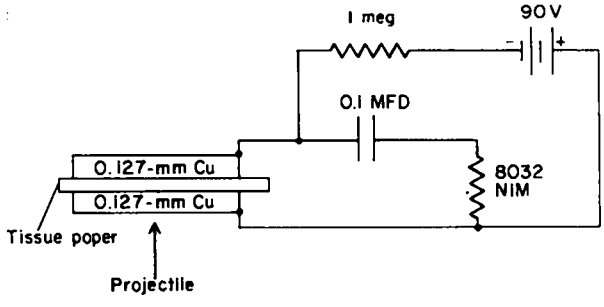

Fig. 2.
PHERMEX trigger circuit.

Another interesting observation can be made by comparing Figs. 3d and 6c, which show tungsten and soft U-0.75 wt% Ti penetrators, respectively, at 150-μs delay. Both penetrators had an incident velocity of 971 m/s. First, the amount of tungsten alloy adhering to the front of the penetrator is significantly greater so the armor has a larger cross section to work against and can offer more resistance to penetration. Also, approximately 10% more of the uranium alloy penetrator remains after an equal amount of armor penetration. Hence, the uranium alloy should have a lower protection ballistic limit (PBL), and it actually does, by about 60 m/s. Careful comparison of the hard and soft uranium alloy penetrators shows that slightly less material may adhere to the hard penetrator on the average, but the difference is quite small.

Figures 4e and 6d illustrate another interesting point. These radiographs of hard and soft U-0.75 wt% Ti penetrators just after penetration clearly show the advantage of the softer, more ductile material that provides a larger fragment behind the armor.

The PHERMEX radiographs provide further information on the penetration process. In particular, one can ascertain the trajectory of the back of the penetrator, the penetrator length, and the penetration depth as functions of time. If the projectile velocities in successive shots had been more accurately controlled, these data would have less scatter. However, the reproducibility is good enough to make the measurements worthwhile and to illustrate the important features. We address the following questions.

How rapidly does the penetrator decelerate?

What is the nature of the "penetration" trajectory?

What is the penetrator erosion history?

Obviously, these phenomena are interrelated.

The quantities measured for each experiment (within the precision of edge definition) were:

a. 20-μs delay; v = 981.1 m/s.

b. 50-μs delay; v = 961.3 m/s.

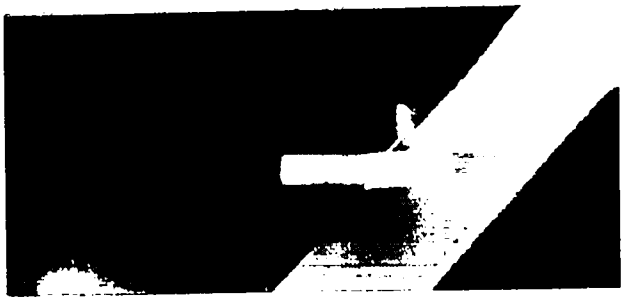

c. 100-μs delay; v = 971.6 m/s.

d. 150-μs delay; v = 971.6 m/s.

e. 200-μs delay; v = 973.8 m/s.

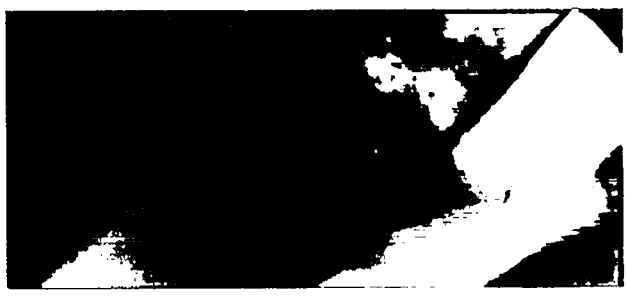

f. 275-μs delay; v = 969.5 m/s.

g. 325-μs delay; v = 981.1 m/s.

Fig. 3.
Penetration shots with tungsten penetrators.

a. 50-μs delay; v = 907.0 m/s.

b. 100-μs delay; v = 945.4 m/s.

c. 150-μs delay; v = 967.7 m/s.

d. 275-μs delay; v = 945.4 m/s.

e. 325-μs delay; v = 946.7 m/s.

f. 421-μs delay; v = 952.4 m/s.

Fig. 4.
Penetration shots with hard U-Ti penetrators.

X_b, the position of the back of the penetrator,
X_f, the position of the front of the penetrator, and
L, the penetrator length.

These data are presented, together with shot numbers and initial projectile velocities, rounded off to three significant figures, in Table II. These data are also presented graphically in Fig. 8 in which the front and back positions of the penetrators and their lengths are plotted as functions of time. The data points are connected by smooth curves.

The most striking feature of the curves is the fact that, within the precision of the data, the velocity of the back of the penetrator remains virtually constant during approximately the first 150 μs of penetration and then drops very rapidly over the next 100 μs. Furthermore, it is not coincidental that the plug sheared from the armor forms during the rapid deceleration of the penetrator. The point is that if the plug were not forming, the penetrator would be defeated almost immediately.

a. 20-μs delay; v = 896.4 m/s.

b. 100-μs delay; v = 893.0 m/s.

c. 150-μs delay; v = 893.9 m/s.

d. 250-μs delay; v = 914.4 m/s.

Fig. 5.
Nonpenetration shots with hard U-Ti penetrators.

Notice that during the first 50 to 100 μs the projectile length is being reduced at a rate that is greater than its penetration velocity. During this time, the back end of the projectile proceeds at nearly constant velocity because only the yield strength of the material can be transmitted to it, and that only at the "bar sound speed" (the square root of Young's modulus divided by density). The stress at the projectile tip is, however, very great at this time because it includes the hydrodynamic contribution from stopping or slowing the tip material. The situation changes relatively abruptly, because as the projectile length is reduced the relative effect of the yield strength increases and the acoustic signal transit time is reduced rapidly. Very soon thereafter, the projectile's residual velocity becomes inadequate to produce enough hydrodynamic pressures to cause either projectile or target material to flow away from the collision zone against the restraining stresses supplied by the armor's strength. Unless the penetration at this time is sufficient to reduce the shear strength of the material around the potential "plug" of armor to a level such that the residual kinetic energy can supply the required plastic work to shear out the plug, the projectile is defeated. It is probably at this stage of penetration that the difference between a "mushroomed" projectile tip like that of the tungsten alloy and a relatively smaller diameter such as the U-Ti presents becomes most important. (Refer again to Figs. 3d and 6c.) At this stage, the diameter of the required plug in the armor is pitted against the total energy remaining in the projectile. This diameter enters in two ways. The shear energy has already been mentioned. In addition, the mass in the plug must be accelerated so that the plug and the residual projectile material have a common velocity. In the Appendix, we present an elementary mathematical model that illustrates some of the above points.

B. Chemical Analyses and Metallography

The LASL Analytical Chemistry Group analyzed the two U-0.75 wt% Ti alloys, using wet analytical procedures to determine the concentration of the principal elements and a quantitative spectrographic analysis to determine trace-element concentrations. Table III shows the results.

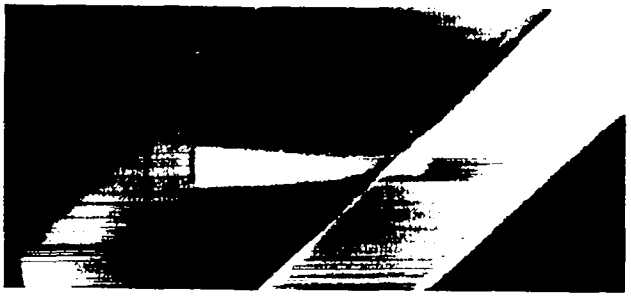

a. 50-μs delay; v = 957.3 m/s.

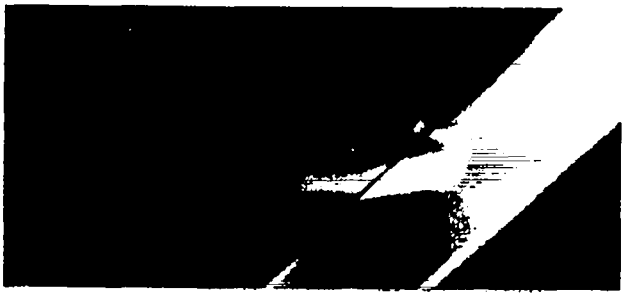

b. 100-μs delay; v = 965.6 m/s.

c. 150-μs delay; v = 970.7 m/s.

d. 275-μs delay; v = 978.1 m/s.

e. 325-μs delay; v = 984.2 m/s.

Fig. 6.
Penetration shots with soft U-Ti penetrators.

Metallography of the hard and soft uranium alloy penetrators was performed by the LASL Materials Technology Group. They sectioned one sample of each penetrator material longitudinally and transversely and examined it metallographically. During metallographic preparation of the samples, centerline quenching voids were discovered. Micrographs of these voids are shown as Fig. 9. It is known that these voids can occur when the diameter of the quenched section is approximately 25.4 mm or greater.

We found the microstructure of the hard U-0.75 wt% Ti to be representative of U-0.75 wt% Ti aged to peak hardness. Figure 10 shows longitudinal and transverse sections. We found the hardness of this penetrator to be 570 DPH. We also noted excessive carbide precipitate in this sample (Fig. 10 left).

The microstructure of the soft U-0.75 wt% Ti was typical of U-0.75 wt% Ti that has not been aged to peak hardness. Figure 11 shows longitudinal and transverse sections. We found the hardness of this material to be 470 DPH.

Fig. 7.
Nonpenetration shot with soft U-Ti penetrator. 100-μs delay; v = 940.6 m/s.

IV. CONCLUSIONS

One conclusion to be drawn from these observations is that the best penetrator should be a simple right circular cylinder with the maximum practical aspect ratio for a given mass. The mass should be chosen so that the velocity is maximum for a given launch capability. These considerations cannot be expected to apply to extreme cases, but they should surely be applicable to variations of about 50% around the length of the present projectiles. Evidently if the projectile diameter is reduced too much, the bending moment will be too small. One might also suspect that the hydrodynamic penetration mechanism might become less efficient, because the armor's strength is fixed whereas the rest of the hydrodynamics scales.

Our second conclusion is that there is apparently an optimum combination of material properties that will give maximum penetration capability and maximum final fragment size. The tungsten alloy was too ductile, and the hard U-Ti alloy was too brittle. Although the soft U-Ti alloy may not be the ultimate choice, it is certainly the best of the three.

Our third conclusion, which may be of considerable importance, concerns the residual velocity of a projectile that has succeeded in penetrating and, thus, the potential damage it can do to objects behind the armor. The data presented here were obtained with projectiles fired at velocities near the PBL, so the residual velocity was small. Figures 8a and 8b, in particular, show, however, that the most rapid projectile deceleration occurred just before final penetration. One would therefore expect that if the initial velocity is increased slightly above the PBL, the residual velocity after penetration will increase in much greater proportion. Put another way, the evidence indicates that the residual velocity is very sensitive to the exact amount of armor penetrated (in a narrow range around the PBL). This fact should have military significance.

TABLE II

PROJECTILE POSITION VS TIME

The time zero is the initial collision. The space zero is the impact surface of the plate, and the space coordinate is measured positive into the plate along the direction of penetration.

Shot	T (μs)	X_{Back} (cm)	X_{Front} (cm)	Length (cm)	V_0 (m/s)
		Tungsten Alloy Penetration Shots			
1546	20	−10.17	1.00	11.25	981
1556	50	− 7.66	2.25	9.75	961
1540	100	− 3.42	3.84	7.17	971
1547	150	+ 1.50	6.08	4.58	971
1541	200	+ 4.38	7.29	2.92	974
1545	275	+ 5.50	8.58	2.75	970
1550	325	+ 6.10	8.40	2.30	981
		Hard U-Ti Penetration Shots			
1551	50	− 7.80	2.15	9.92	907
1543	100	− 2.67	4.75	7.25	945
1561	150	+ 1.25	6.42	5.25	968
1548	275	+ 7.92	10.58	2.67	945
1562	325	+11.00	12.50	1.50	947
		Hard U-Ti Nonpenetration Shots			
1552	20	−10.50	0.75	11.25	896
1563	100	− 3.33	4.50	7.75	893
1553	150	+ 0.10	6.00	5.60	894
1554	250	+ 6.41	8.58	2.17	914
		Soft U-Ti Penetration Shots			
1555	50	− 7.08	2.58	9.83	957
1557	100	− 2.50	5.00	7.50	966
1558	150	+ 1.83	6.91	5.08	971
1559	275	+ 9.25	12.50	3.25	978

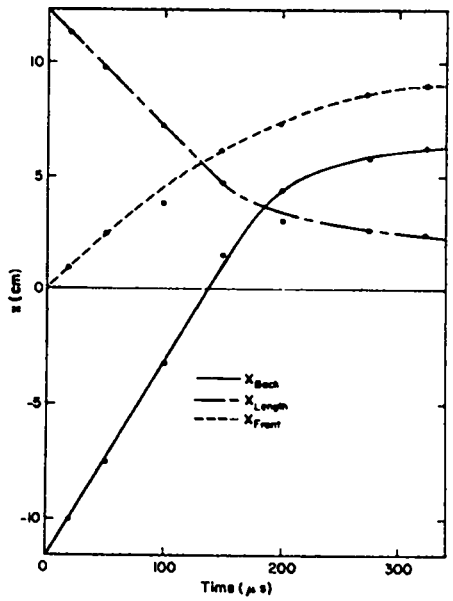

a. *Tungsten alloy penetration shots.*

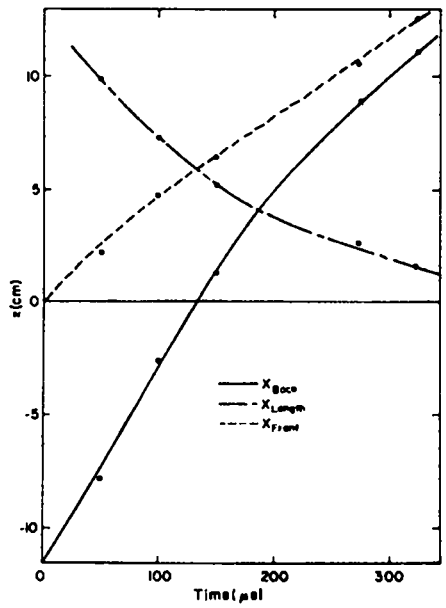

b. *Hard U-Ti penetration shots.*

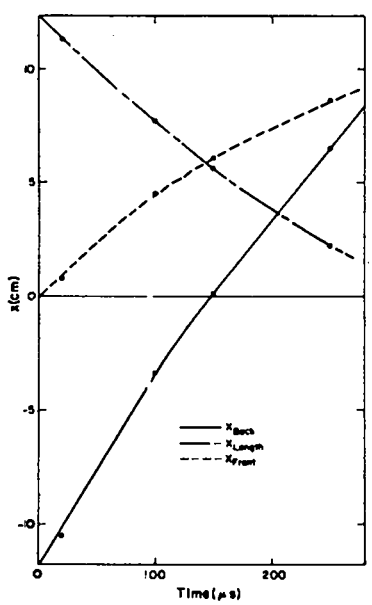

c. *Hard U-Ti nonpenetration shots.*

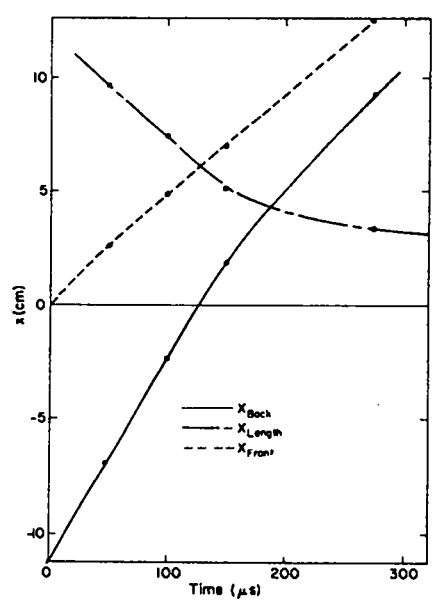

d. *Soft U-Ti penetration shots.*

Fig. 8.
Position vs time for the front (X_F) and back (X_B) ends and the lengths (X_L) of projectiles used in shots at PHERMEX.

TABLE III

CHEMICAL ANALYSIS OF U-0.75 WT% TI

Element	Concentration in Hard Alloy	Concentration in Soft Alloy
Ti	0.85 wt%	0.75 wt%
C	40[a]	45
N	25	15
H_2	32	8
O_2	65	45
Li	<0.2	<0.2
Be	<0.2	<0.2
B	<0.2	<0.2
Na	1	<1
Mg	4	<1
Al	30	>0
Si	60	>0
P	<120	<120
Ca	<6	<6
V	<60	<60
Cr	2	2
Mn	6	18
Fe	120	120
Ni	120	60
Cu	300	35
Zn	<30	<30
Sr	<50	<50
Mo	350	<60
Ag	<1	<1
Cd	<1	<1
Sn	6	<2
Sb	<6	<6
Ba	<6	<6
Pd	<2	<2
Bi	<2	<2

[a]All values are in parts per million unless otherwise noted.

ACKNOWLEDGMENTS

We acknowledge the valuable assistance provided by various groups and individuals within LASL. In particular we thank W. E. Deal of the LASL M Division Office and E. H. Eyster of the WX Division Office for their critical review of the manuscript. Group CMB-1 is acknowledged for sample analysis, and Group CMB-6 is acknowledged for metallographic analysis of the samples. We especially thank M. L. Brooks, WX Division Office, for technical and administrative guidance.

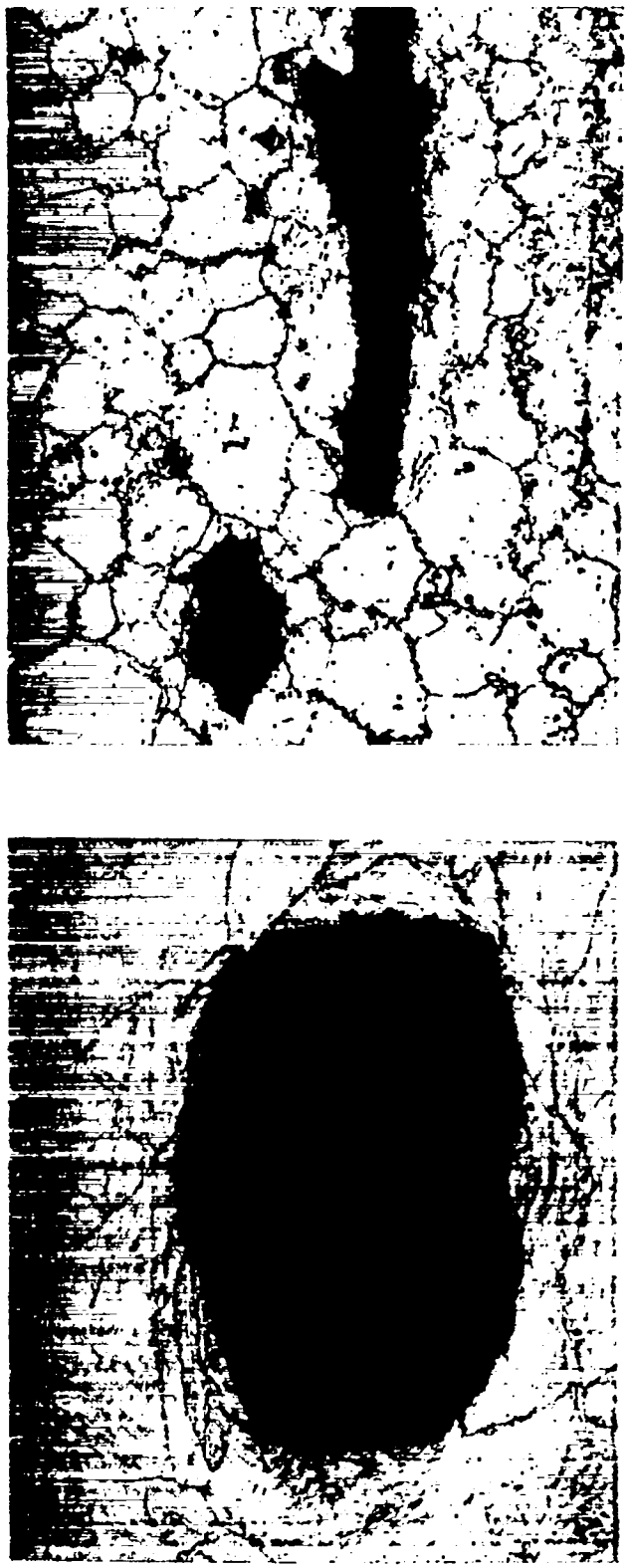

Fig. 9.
Centerline voids in hard U-0.75 wt% Ti (top) and in soft U-0.75 wt% Ti (bottom).

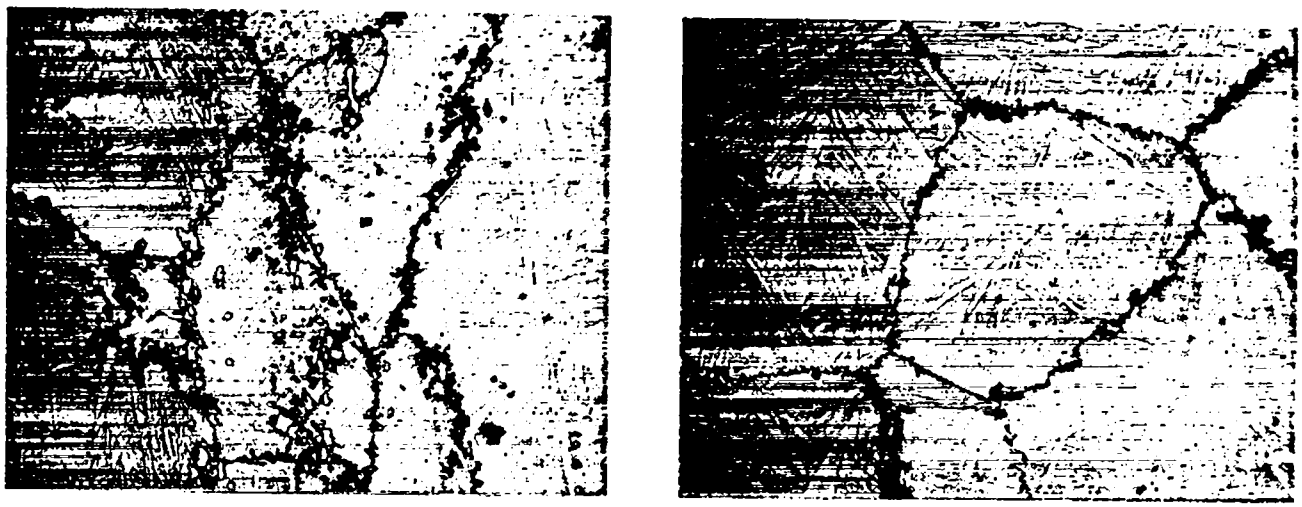

Fig. 10.
Photomicrographs of hard U-0.75 wt% Ti. 250 X. Left: longitudinal section. Right: transverse section.

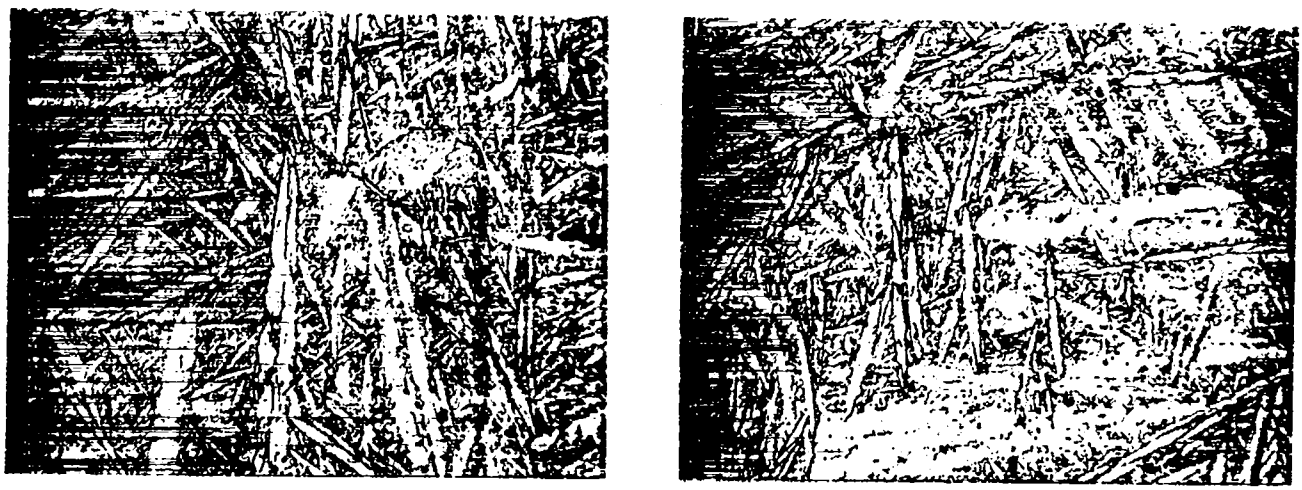

Fig. 11.
Photomicrographs of soft U-0.75 wt% Ti. 250 X. Left: longitudinal section. Right: transverse section.

APPENDIX

ELEMENTARY MODEL OF EARLY STAGE PENETRATION

Complete analytical modeling of the penetration process in experiments like those discussed here is, of course, very complicated. It is perhaps useful, however, to consider a much simplified but qualitatively fairly accurate model of the important features.

Visualize a right circular cylinder of material of density ρ, length L, dynamic yield strength σ_y, and velocity v, which strikes another material whose mass we consider infinite. We assume that the entire length, L, is subjected to the retarding stress, σ_y. This is not a bad approximation after one acoustic signal transit time. The deceleration of the cylinder is

$$\frac{\rho L dv}{dt} = -\sigma_y \qquad \text{(A-1)}$$

except in a very narrow zone near the collision plane. We shall ignore this zone. If the instantaneous

velocity of the collision plane (because of simultaneous erosion of the projectile and the target) is V, the time rate of change of L is

$$\frac{dL}{dt} = -(v - V) , \qquad \text{(A-2)}$$

when all ejected material flows out of the collision zone.

In the early stages of penetration, before the armor begins to bulge and the plug begins to form, $V = kv$, where k is a constant less than unity. In fact, Fig. 8 shows that $k \approx 0.5$. Assume this to be true indefinitely. We shall now calculate the trajectory of such a projectile into infinitely thick armor. Using $v - V = 0.5\,v$ in Eq. (A-2) and dividing Eq. (A-1) by (A-2), we have

$$\frac{0.5\,\rho L v dv}{dL} = -\sigma_y \qquad \text{(A-3)}$$

with the solution

$$L = L_0 e^{-\frac{\rho(v_0^2 - v^2)}{4\sigma_y}} \qquad \text{(A-4)}$$

where

L_0 = initial length of projectile,
v_0 = initial velocity of projectile.

The first interesting result is that the final residual length of the stopped projectile is

$$L_\infty = L_0\, e^{-\frac{\rho v_0^2}{4\sigma_y}} \qquad \text{(A-5)}$$

Assuming that

$L_0 = 11.4$ cm,
$\rho = 18$ g/cm^3,
$v_0 = 9 \times 10^4$ cm/s,
$\sigma_Y = 20$ kbar,

we calculate that $L_f = 1.84$ cm, which is exactly the sort of value we observe.

To find the length as a function of time, we rewrite Eq. (A-4) in the form

$$v = -2\frac{dL}{dt}\sqrt{v_0 + \frac{4\sigma_y}{\rho}\ln L/L_0} \qquad \text{(A-6)}$$

and integrate it numerically. Figure A-1 shows the length vs time for the set of parameters used in the above calculation. Obviously, the predicted behavior is not only qualitatively correct; it is semi-quantitatively correct in the sense that the calculated residual length is within a factor of 2 of those observed experimentally, and the length vs time curve changes slope very abruptly between 150 and 300 μs.

The real questions that would have to be answered to construct a more accurate theory are, principally:

What determines the ratio of the projectile's erosion rate to that of the target?

What are the details that finally cause a finitely thick target to form a shear plug?

Further thought along these lines might lead to a way of selecting the combination of projectile aspect ratio, mass, and velocity that would give maximum penetration with a maximum residual fragment.

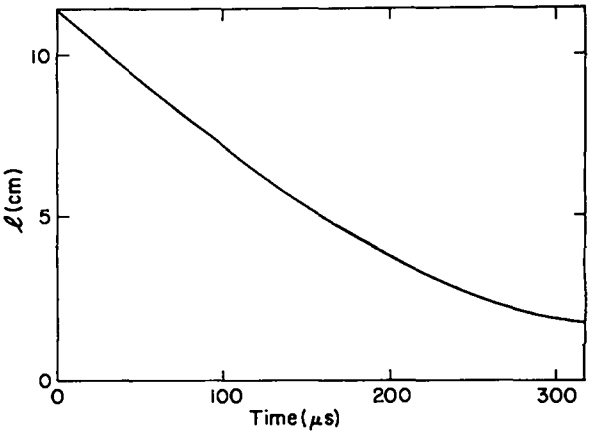

Fig. A-1.
Calculated length vs time for the projectile described in the Appendix.